Version of Record: https://www.sciencedirect.com/science/article/pii/S0960077919300943
Manuscript_3aee7a3b4d4dad860616bedda1d9634d

Nonlinear Dynamics of an Origami Wheel with Shape Memory Alloy Actuators

Larissa M. Fonseca [1]
Guilherme V. Rodrigues [1]
Marcelo A. Savi [1]
Alberto Paiva [2]

[1] Center for Nonlinear Mechanics
COPPE – Department of Mechanical Engineering
Universidade Federal do Rio de Janeiro
21.941.972 – Rio de Janeiro – RJ, Brazil, P.O. Box 68.503
Email: larissamaciel.lah@gmail.com; guilherme_@live.co.uk; savi@mecanica.ufrj.br

[2] Department of Mechanical Engineering
Universidade Federal Fluminense
27.255.250 – Volta Redonda – RJ, Brazil
Email: paiva.ufrj@gmail.com

ABSTRACT

Origami generates three-dimensional structures from two-dimensional sources and is inspiring engineers to design systems related to different applications as robotics, biomedical and aerospace engineering. The use of smart materials increases the range of applicability of origami systems exploiting adaptive behavior. In this regard, shape memory alloy (SMA) actuators are being used to promote geometrical changes in origami structures. This paper deals with the nonlinear dynamics of an origami wheel with SMA actuators. The origami wheel has strong geometric and constitutive nonlinearities presenting a complex dynamical response. Symmetry assumptions related to waterbomb folding pattern allow one to develop a single degree of freedom reduced-order model system that describes origami dynamics. Based on that, numerical simulations are carried out representing different operational conditions presenting a general comprehension of the origami dynamical response. Origami complex behavior is of concern showing chaotic motions and strong parameter sensitivity.

Keywords: Origami; shape memory alloys; self-expandable structures; nonlinear dynamics; chaos.

1 INTRODUCTION

Origami is the art of paper folding being one of the oldest popular Japanese art. In brief, this is the art of creating sculpture representation from a flat paper sheet. Therefore, it produces a 3D structure through some folding pattern of a 2D source. Mathematicians provided the first formal origami non-artistic point of view, introducing geometric proofs and analysis. The first description of the origami geometric construction was given by Huzita (1989), which introduced six axioms showing details about folding patterns. It was discussed the existence and, in some cases, uniqueness to create a single crease on a sheet of paper attending some restrictions, such as the connection between specific points.

Recently, origami is inspiring the construction of self-foldable, compact, adaptive systems and devices for various fields of science and technology (Peraza-Hernandez *et al.*, 2014; Fei & Sujan, 2013). Classical shapes as spheres and cylinders or some combination of folded shapes can be exploited assuming forms between different configurations, being useful for different purposes. This general idea can be employed on architectural design (Sorguç *et al.*, 2009), robotics (Felton *et al.*, 2014), aerospace systems (Nishiyama, 2012) and biomedical devices (Salerno *et al.*, 2014).

The use of smart materials provides actuation of origami systems, exploiting different physical field coupling. Basically, external fields as temperature, electric or magnetic field can induce the origami shape alteration between desired configurations. Shape memory alloys (SMAs) and magnetic materials are of special interest due to their capacity to generate forces and displacements (Savi *et al.*, 2016).

Pesenti *et al.* (2015) studied origami kinematic behavior, aiming its application in adaptive frontage with solar skin. Origami-folding patterns are exploited and potential application of deployable solar shading devices with SMA actuation is investigated evaluating the environmental changing conditions.

Miyashita *et al.* (2015) fabricated a thermal activated self-folding sheet that is part of a miniature origami robot controlled by an external magnetic field. This 3D untethered robot can accomplish some basic tasks like walking, swimming, digging, climbing a slop, carrying blocks and can even be dissolved in a solvent, depending on the origami composition. Kuribayashi *et al.* (2006) developed a new type of stent graft made from foldable NiTi foil. This design allows one to obtain closed-opened cylindrical configurations with thermal actuation.

Origami folding process can be analyzed from different approaches, depending on the desired description. Lang (1996; 2011) made an arithmetic description of origami using tree theory,

and its corresponding computer program, by converting the problem of finding an efficient origami crease pattern into one of several types of nonlinear constrained optimization. Belcastro & Hull (2002) discussed a mathematical description of some general folding processes by affine transformations, modeling the folding of a flat paper sheet by examining a map $f: \mathbb{R}^2 \rightarrow \mathbb{R}^3$. For some patterns that can be assembled with repeated unit cells, such as the waterbomb and Yoshimura patterns, closed-form equations can be derived to describe the entire folding process. Nevertheless, purely geometric descriptions can only be used for rigid origami. Idealized rigid origami presents an important advantage in terms of deformation, meaning that the deformation is completely realized by the folding/unfolding at the creases and does not involve any deformation at the rigid faces (Ly *et al.,* 2014). Liu & Paulino (2017) developed an interesting study on non-rigid origami, proposing a general nonlinear formulation for structural analysis of origami elements. They made a general bar-and-hinge model that also considers some banding on the faces.

The material employed for origami construction is another important subject related to general applications. Paper and polyester are both easy to obtain and fold and are often used to prototype origami folding patterns. Nevertheless, they can present some disadvantages. Paper can tear easily, has a low fatigue life and has low shear strength. Polyester does not tear easily and has a fatigue life of 10^6 cycles (DuPont Films, 2003). In this regard, the use of other materials is related to some techniques employed to generate foldable structures. Smart Composite Manufacturing (SCM) is a process that creates foldable laminates from laser micromachined layers of carbon fiber and polymers (Merz *et al.*, 1994). These techniques can increase the fatigue life or just improve the material strength, allowing one to carry more weight, support withstand greater forces or to resist to greater shear stresses.

Since origami systems are slender structures, they are usually close to stability limits with important dynamical issues to be investigated. The combination of strong geometrical nonlinearities associated with origami patterns, and constitutive nonlinearities related to smart material actuators, is responsible for a rich dynamical behavior. Operational excitations can affect the system response being critical to several applications. Therefore, dynamical response of origami systems is of special importance during design stage. Nevertheless, dynamical behavior of origami systems is only treated in few references in literature (Rodrigues *et al.*, 2017) and this article has this main goal.

This paper deals with the dynamical analysis of an expandable origami wheel that exchange between different configurations due to thermal actuation provided by SMA actuators (Figure 1). The origami wheel is built based on the waterbomb pattern and its application has advantages for robotics applications. Trajectory changes by wheel configuration changes, obstacle overcomes, and roll movement stabilization are some examples. Origami geometric relations are established

defining a single-degree of freedom reduced-order model, exploiting origami symmetry. Dynamical modeling considers a polynomial constitutive theory (Falk, 1980) to describe the SMA thermomechanical behavior. Numerical simulations are carried out showing different operational conditions. Complex dynamical behavior is treated showing chaos and dynamical jumps.

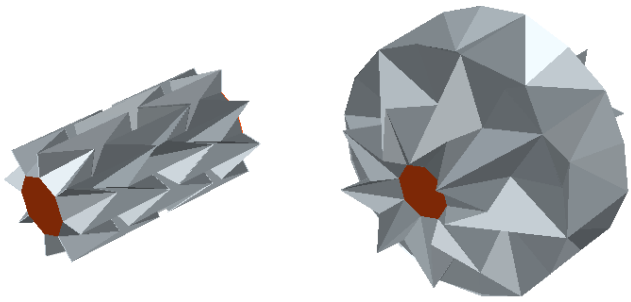

Figure 1: Origami wheel showing two limit configurations.

2 ORIGAMI WHEEL

Origami wheel is constructed employing a 3×8 magic-ball or waterbomb pattern, which has been used in various applications (Ma & You, 2014). Waterbomb pattern can be considered as a rigidly foldable or rigid origami that consists of panels that can move continuously between folded configurations by rotating around the crease lines without deformation. A planar version of the waterbomb pattern, Figure 2, can be bent producing a cylindrical-type structure. Figure 2 also presents two configurations of the unit cell of the origami pattern.

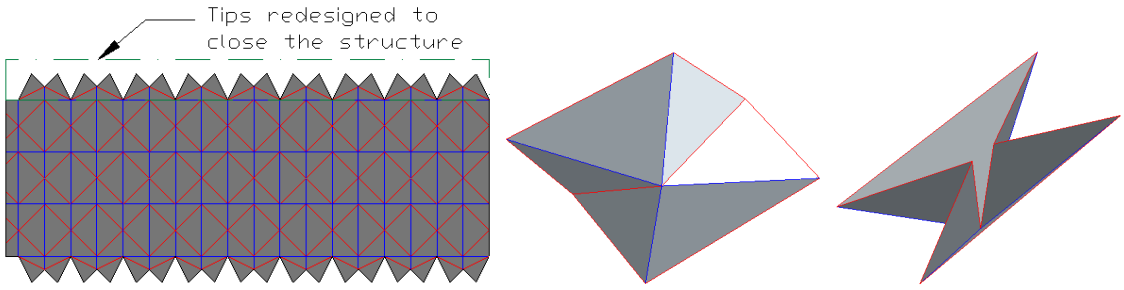

Figure 2: The waterbomb pattern (3 layers ×8 cells by layer) employed to create the origami wheel (left) and two unit cell configurations. Blue line means valley fold and red line means mountain fold.

The main point of the use of an origami wheel is to create an expandable structure that can alter its configuration from some external stimulus. Specifically, the idea is to use SMA springs placed on the origami circumferential direction, which can be thermal actuated to promote

configuration exchanges. Besides these SMA actuators, the system needs a passive bias elastic spring, placed in the longitudinal direction, ensuring the shape change of all the structure between two limit configurations. Figure 3 shows origami wheel with SMA springs and passive elastic spring connected to acrylic plates at the ends of the wheel. It should be pointed out that the SMA is attached to the origami middle layer, highlighted at the planar version, referred as *middle column*.

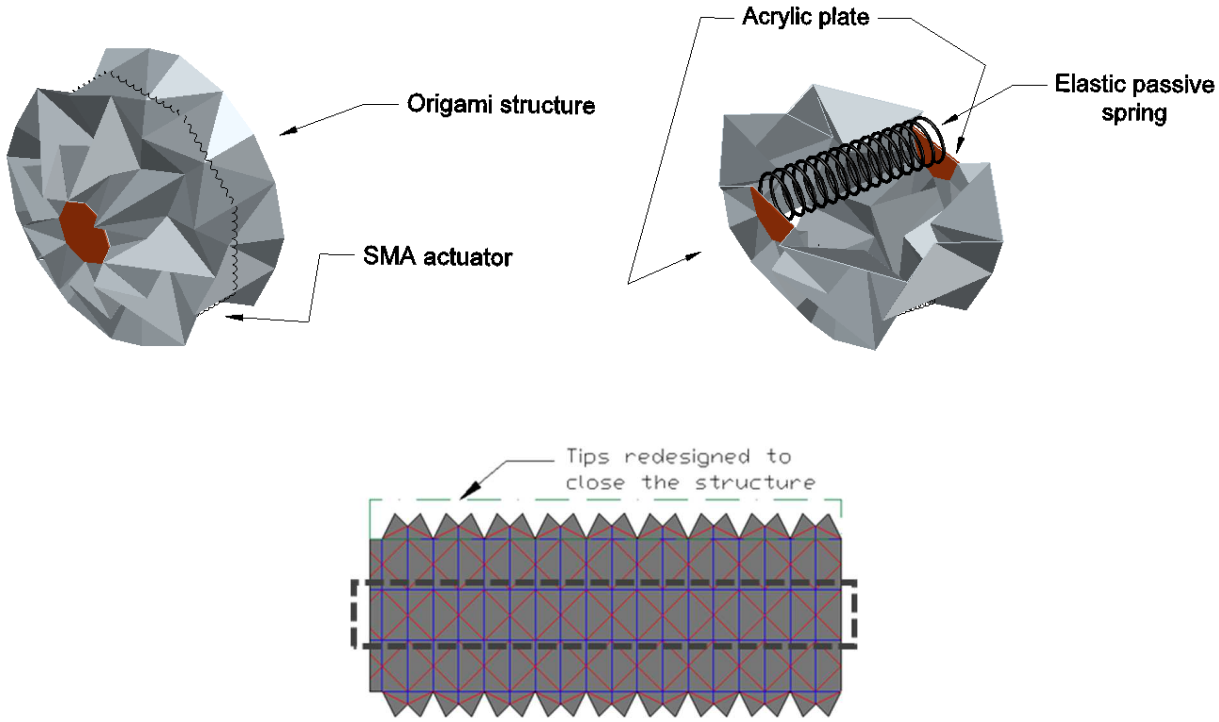

Figure 3: Origami wheel with shape memory alloy actuators (superior panel, left) and a view with the bias elastic spring (superior panel, right). Planar view showing the middle column (inferior panel).

The concept of the origami wheel functioning is based on SMA remarkable properties due to austenite-martensite solid phase transformation that can be induced either by stress or temperature changes. Typically, SMAs present two main thermomechanical behaviors: pseudoelasticity and shape memory effect. Pseudoelasticity is a typical high temperature behavior where stress induced phase transformations cause large strains and hysteretic behavior (Figure 4-a). On the other hand, shape memory effect is the one where a mechanical load induces phase transformations that cause a residual strain that can be recovered by a thermal loading process (Figure 4-b). The bias system composed by the SMA spring in opposition with an elastic spring is characterized to promote a two-way system where the elastic spring produces the mechanical load necessary for the reverse movement, recovering the initial displacement of the SMA spring (Figure 4-c).

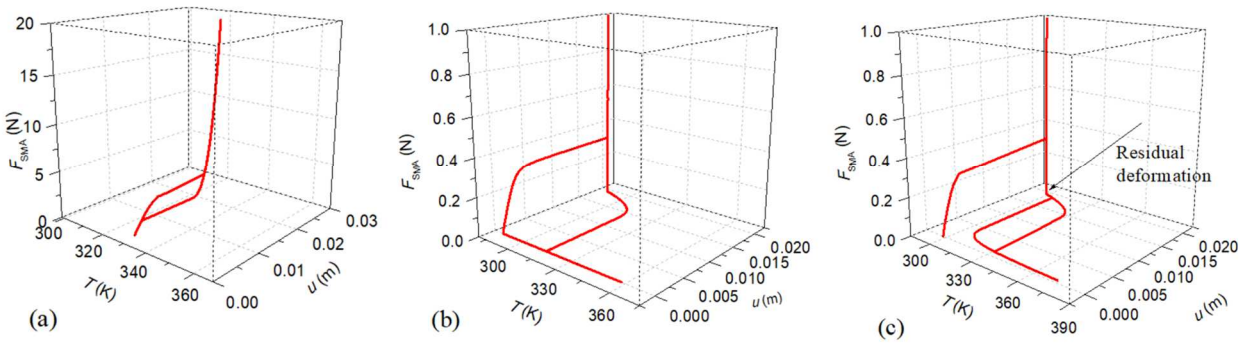

Figure 4: SMA typical force-displacement-temperature curves: (a) pseudoelastic effect; (b) shape memory effect; (c) shape memory effect on a bias system composed by an SMA in opposition with an elastic spring.

The origami wheel actuation is a bias system with an SMA spring against an elastic spring, exploiting the shape memory effect. It is designed in such a way that a previous training process induces a residual strain being associated with detwinned martensite. The actuator is then placed in the origami, with a bias elastic spring. Under this condition, the heating of the SMA actuators induces a martensitic-austenitic phase transformation, increasing its stiffness and recovering the residual deformation (reducing the length of the spring), and promoting the wheel configuration change. On the other hand, when it is cooled, the passive elastic spring acts by pulling the wheel in the longitudinal direction, recovering its initial radius and inducing the reverse phase transformation that decreases the stiffness. Figure 5 shows a schematic picture presenting the correlation between the macroscopic behavior of the actuation system due to temperature changes and the origami configuration changes.

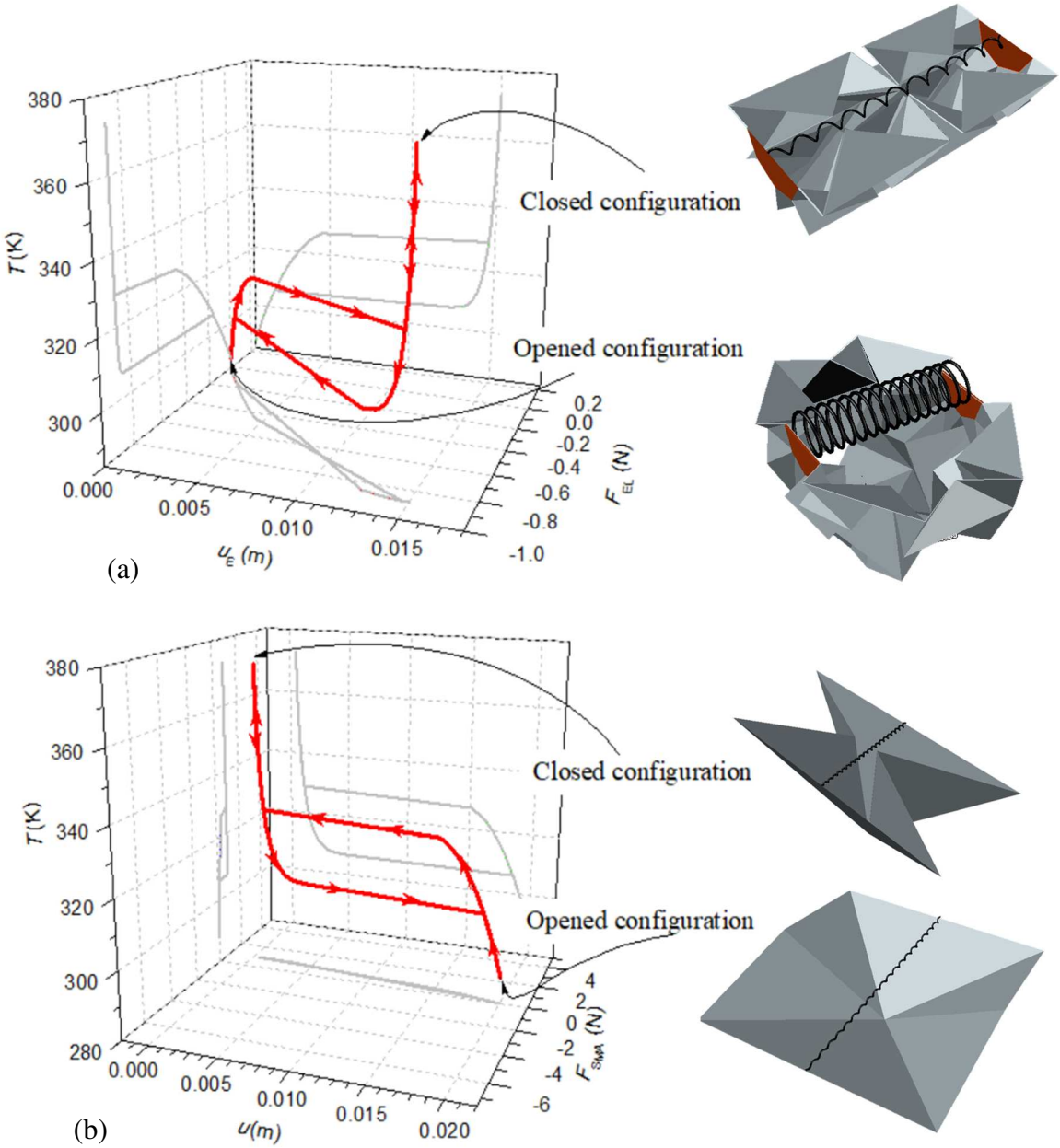

Figure 5:Temperature-displacement-force diagram for a heating/cooling cycle of the origami actuation using SMAs. (a) Diagram for the elastic spring, with opened and closed configurations highlighted. (b) Diagram for the SMAs, with opened and closed configurations highlighting a unit cell.

2.1 Shape changing and symmetry hypothesis

Waterbomb pattern assumes that all folding process occurs only on the creases, and the panels remain flat. When a tessellation is made using this pattern, the whole structure folding process must be previously analyzed to verify if the rigid characteristic remains during the shape changing. Depending on the displacement imposed to the structure, some bending between layers or even in the panels can occur (see Figure 6). The region where this bending is small enough to be

neglected is called rigid-foldability region (the range of values at which the panels remains as a rigid body). Based on origami rigid-foldability hypothesis, displacement paths are related to uniform expansion/contraction with bending between layers (Chen *et al.*, 2016). Fang *et al.* (2017) developed a kinematic study of a 3×8 origami wheel structure folding process, identifying the rigid-foldability region.

Besides rigid-foldability hypothesis, symmetry conditions can be assumed for geometric and external forces. Based on that, rotational symmetry is observed, being related to axial movement during expansion, meaning that both ends are pulled equally, avoiding snaps on origami sides. Under these assumptions, a single cell is representative of the general origami wheel behavior. There are situations where symmetry conditions are not respected, and Figure 6 shows an asymmetric origami behavior. In this case, side B is collapsed, meaning that there is no axial symmetry and a unit cell is no longer representative of the general origami behavior.

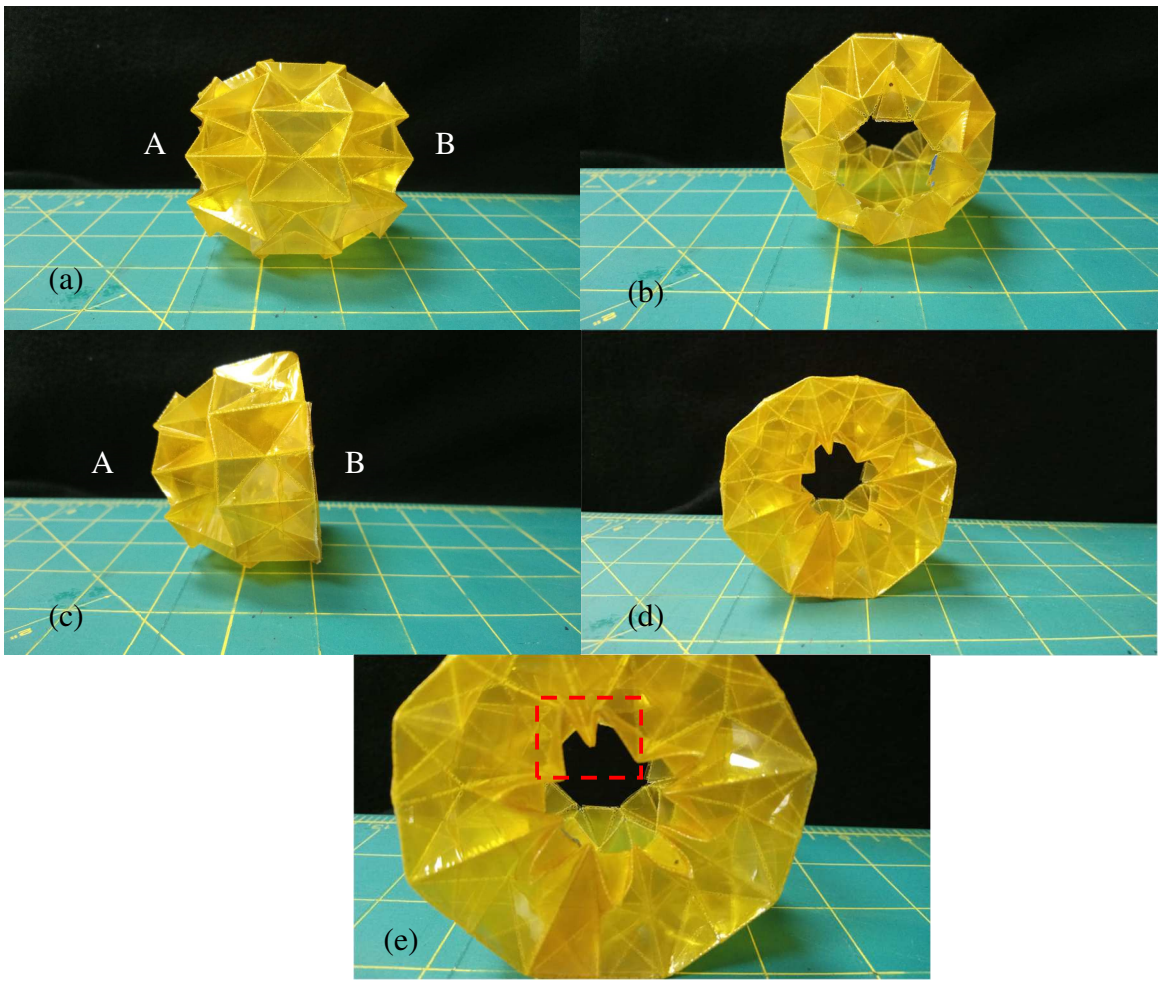

Figure 6: Origami wheel with an asymmetric shape. (a) Structure with symmetric shape on both sides A and B; (b) front view of side B; (c) structure with side B collapsed; (d) front view of side B; (e) zoom of side B where it is possible to see a bending between layers (highlighted by the dashed rectangle).

2.2 Geometrical Analysis

The folding analysis can be modeled by considering an analogous mechanism or a graph representation of a single origami unit cell. Once the origami wheel is a rigid origami, and its range of operation is inside the rigid-foldability region, it can be analyzed as a mobile over-constrained metamorphic mechanism loop, which can change its shape and presents no face deformations. A mechanism is usually characterized by establishing a transformation between an input, such as force or displacement, into an output. A metamorphic mechanism is the one with the ability to change its shape, generating different topologies by reconfiguration.

The analogous mechanism analysis allows one to define the number of inputs required to completely describe the origami, treated as a linkage mechanism, defining the number of degrees of freedom (DOF) also known as the mechanism mobility. The analysis starts considering a linkage mechanism that is representative of an origami unit cell (Chiang, 2000; Chen *et al.*, 2016). Each origami face is represented by a rigid link and joints represent creases (Figure 7).

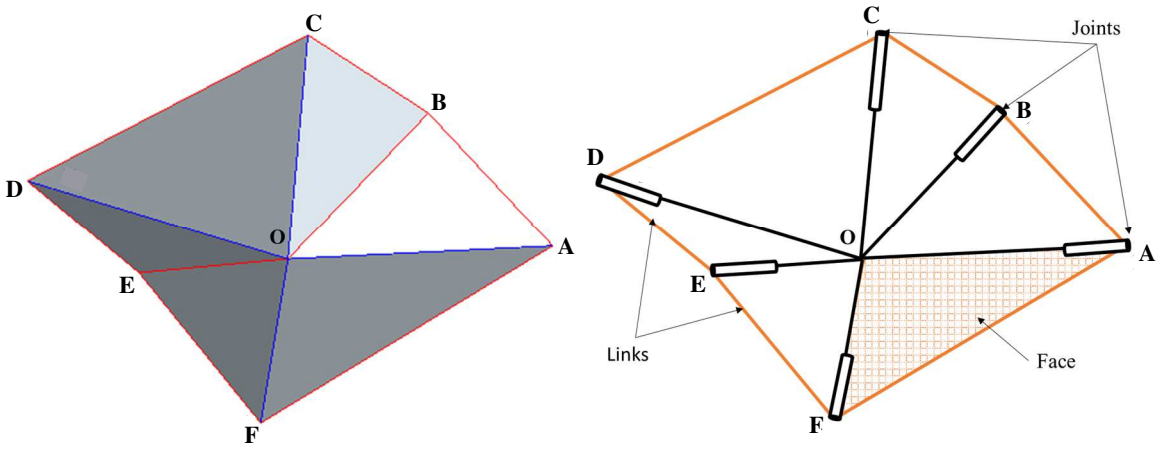

Figure 7: Origami unit cell and mechanism representation considering a mechanism analogy.

The mechanism configuration, or the origami shape, can be completely defined by a required number of inputs or predefined angles between the links. Chebyschev-Grübler-Kutzbach (C-G-K) equation can be employed for this aim (Gogu, 2004). This approach assumes the mechanism construction (joints, links and movements allowed), considering that one link is fixed to an inertial frame. The mobility, M, represents the number of DOF and can be written as a function of the number of links (N), the number of joints (J) and the joint type (planar, spherical, cylindrical). The joint type influences two variables: the generalized displacement of the ith joint, f_i

(i= 1, … J), and the constraint parameter related to the mechanism movement (Λ). Based on that, it is possible to write the following equation,

$$M = \Lambda(N - J - 1) + \sum_{i=1}^{J} f_i \quad (1)$$

The definition of joint type considers three basic forms described in the sequence. A planar mechanism has its motion restricted to the plane, allowing two translational movements and a rotation $\{x, y, \theta_z\}$ (Figure 8-a), which provides a constraint parameter Λ=3. A spherical mechanism has rigid connections with movements restricted to a sphere $\{\theta_x, \theta_y, \theta_z\}$ (Figure 8-b), providing a constraint parameter Λ=3. Finally, a spatial mechanism can translate and rotate in any direction, leading to a constraint parameter Λ=6 (Figure 8-c).

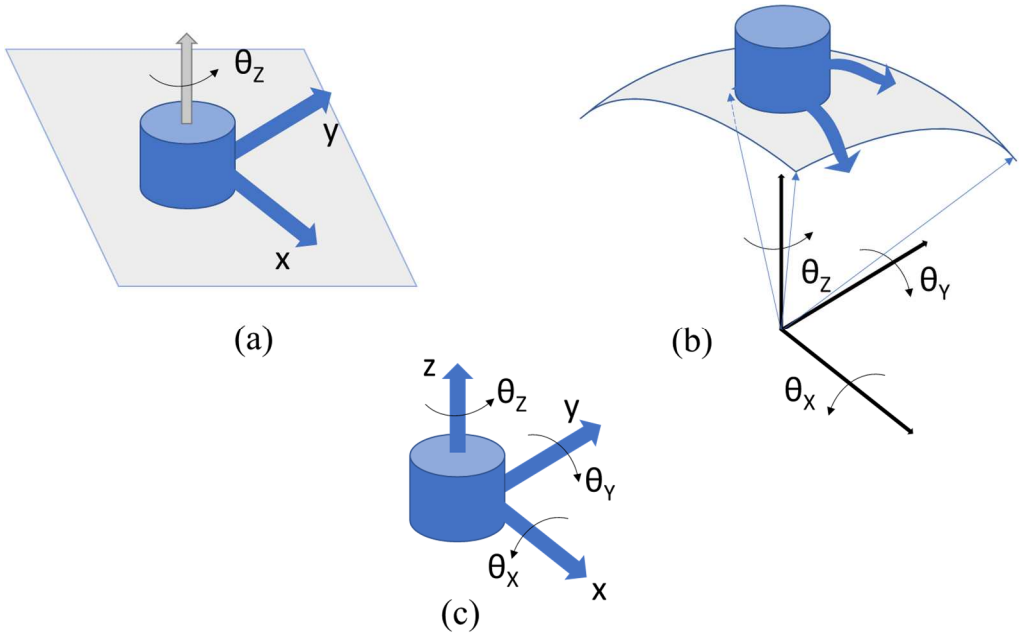

Figure 8: Mechanism movement representation: (a) planar; (b) spherical; (c) spatial.

The waterbomb pattern unit cell is typically a spherical mechanism (Λ=3) with 6 faces or links (N=6) and 6 creases or joints (J=6). Observing Figure 7, it is noticeable that all joints connect to the same point (Point O) and, since all links are rigid, joint movements are restricted. Hence, each joint has only 1DOF (f_i=1), the rotation θ_Z. Therefore, C-G-C equation results M=3, which means that each cell is completely described by 3DOF.

Besides the origami symmetry, the unit cell itself can be considered with symmetric behavior, assuming that diagonal opposite angles have the same value (Bricard line-symmetry) and angles on the same plane have the same value (Bricard plane-symmetry) (Baker, 1980). In this

regard, the following assumptions are adopted: A=C=D=F and B=E. Since this is a closed loop mechanism, these angles have a coupling relation, leading to a 1DOF mechanism. Therefore, the symmetric origami unit cell can be described by 1DOF.

Since the unit cell is a spherical mechanism, it is convenient to employ spherical trigonometry to describe its geometric relations. Figure 9 presents a unit cell and some different views circumscribed in a sphere. Figure 9-a shows the top view of the unit cell while Figure 7-b presents the side view. Figure 9-c shows a tridimensional view while Figure 9-d presents the unit cell assumed to be a rectangle with sides $2a$ and $2b$ and internal acute angle λ, such that $a = b\tan(\lambda)$. By definition, each side of the spherical triangle (spherical arc) is defined by its correspondent internal angle. Thus, the arcs defined by the origami unit cell are known, assuming the values $\widehat{AB} = \widehat{BC} = \widehat{DE} = \widehat{EF} = \lambda$ and $\widehat{CD} = \widehat{FA} = \pi - 2\lambda$.

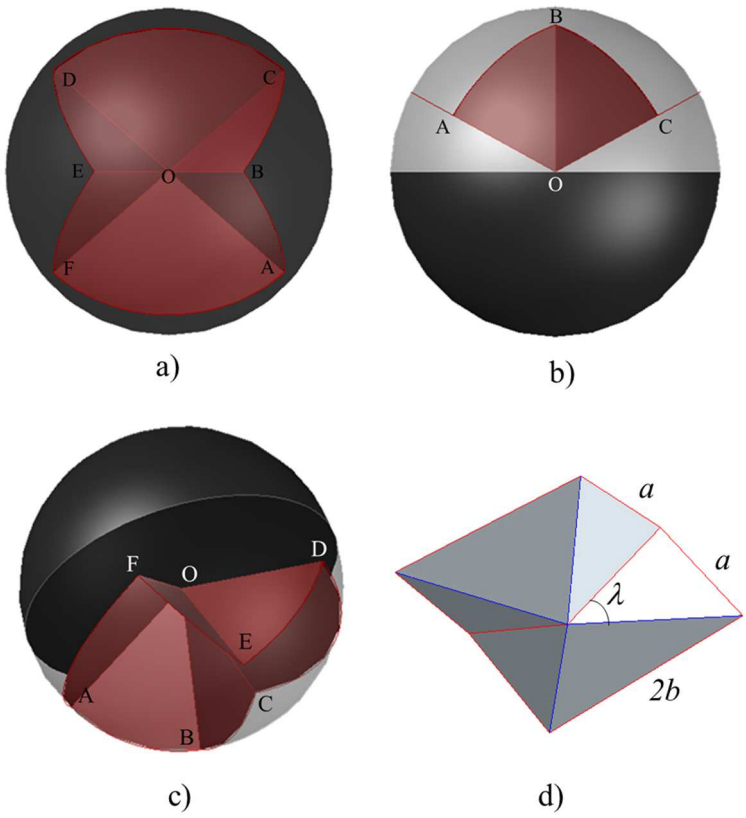

Figure 9: Spherical representation of the origami unit cell: (a) top view; (b) side view; (c) tridimensional view; (d) schematic view of a unit cell.

Since a symmetric behavior is assumed, a quarter of the unit cell is enough to describe the geometric relation. Therefore, two angles are enough to describe the unit cell behavior and it is

chosen θ (angle between faces OAF and OCD) and α (angle between the creases OB and OE). Trigonometric relations on the sphere can define these angles. Figure 10 shows the triangles inside the sphere employed to obtain the unit cell geometric relations, where ϕ_1 is the spherical angle between arcs $\widehat{AB}$ and $\widehat{AC}$ and ϕ_2 is the spherical angle between arcs $\widehat{AF}$ and $\widehat{AB}$. Since only a quarter of the unit cell is analyzed, the point G is defined such that $\widehat{AG} = \widehat{AF}$ and $\sphericalangle BGA = {}^{\pi}/_{2}$. Under these assumptions, and using spherical trigonometry, the following relations are obtained:

$$\phi_1 = 2\theta \tag{2}$$

$$\cos(\phi_2) = \frac{\cos(\theta)\cos(\alpha)}{\sin(\lambda)\cos(\lambda)} - 1 \tag{3}$$

$$\sin(\phi_2) = \frac{\sin(\theta)\cos(\alpha)}{\sin(\lambda)} \tag{4}$$

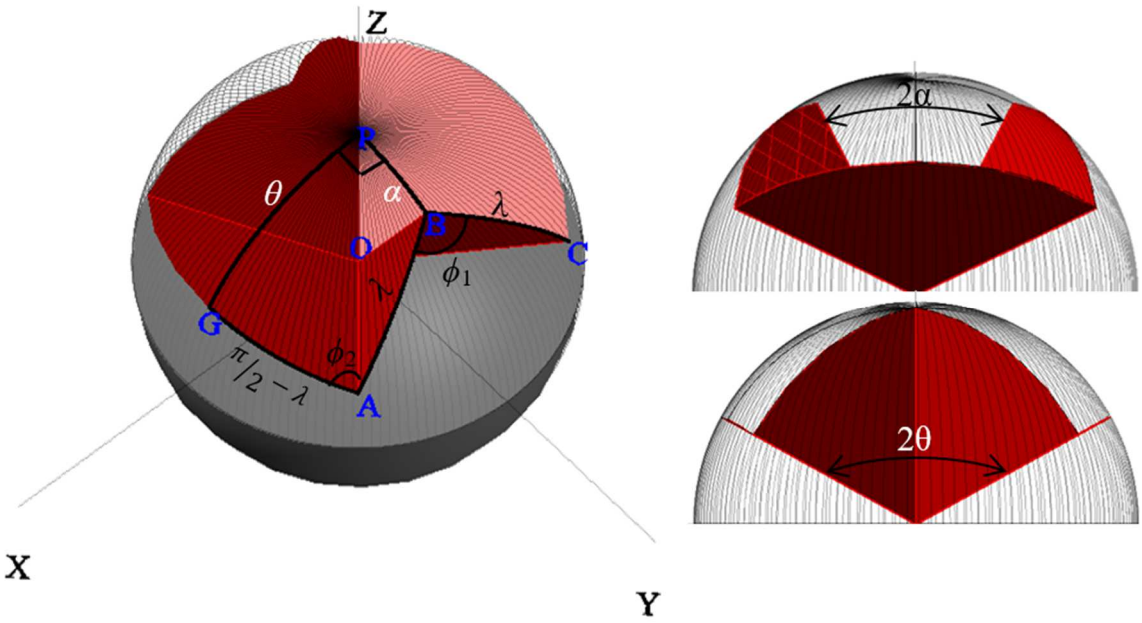

Figure 10: Spherical triangles used to define geometric relations of the unit cell, computing angles α and θ.

Relations (3) and (4) can be manipulated leading to the geometric relation between θ and α for the symmetric behavior of the unit cell:

$$\cos(\theta)\cos(\alpha)\tan(\lambda) + |\sin(\alpha)| = 1 \tag{5}$$

The essential purpose of the origami geometrical analysis is to establish a relation between the unit cell behavior and the origami radius that represents the wheel configuration, allowing the description of the opening and closure process. Origami radius can be defined from two

circumferences starting from the geometric center of the origami wheel. In this regard, it is possible to define an inner radius (red circle at Figure 11), named as the small radius; and an outer radius (dashed blue circle at Figure 11), named as the large radius. They are both related to the middle column or the central region of the origami folding pattern, and can vary with configuration exchanges. This analysis establishes an angle-distance relation obtained from the connection between half-unit cell of the middle column and a half-unit cell on the tip, resulting in a system described by actuators length L_1 (one SMA spring, related to the wheel radius) and L_2 (half-length of elastic passive spring, related to the normal distance the between two acrylic plates), as shown in Figure 11.

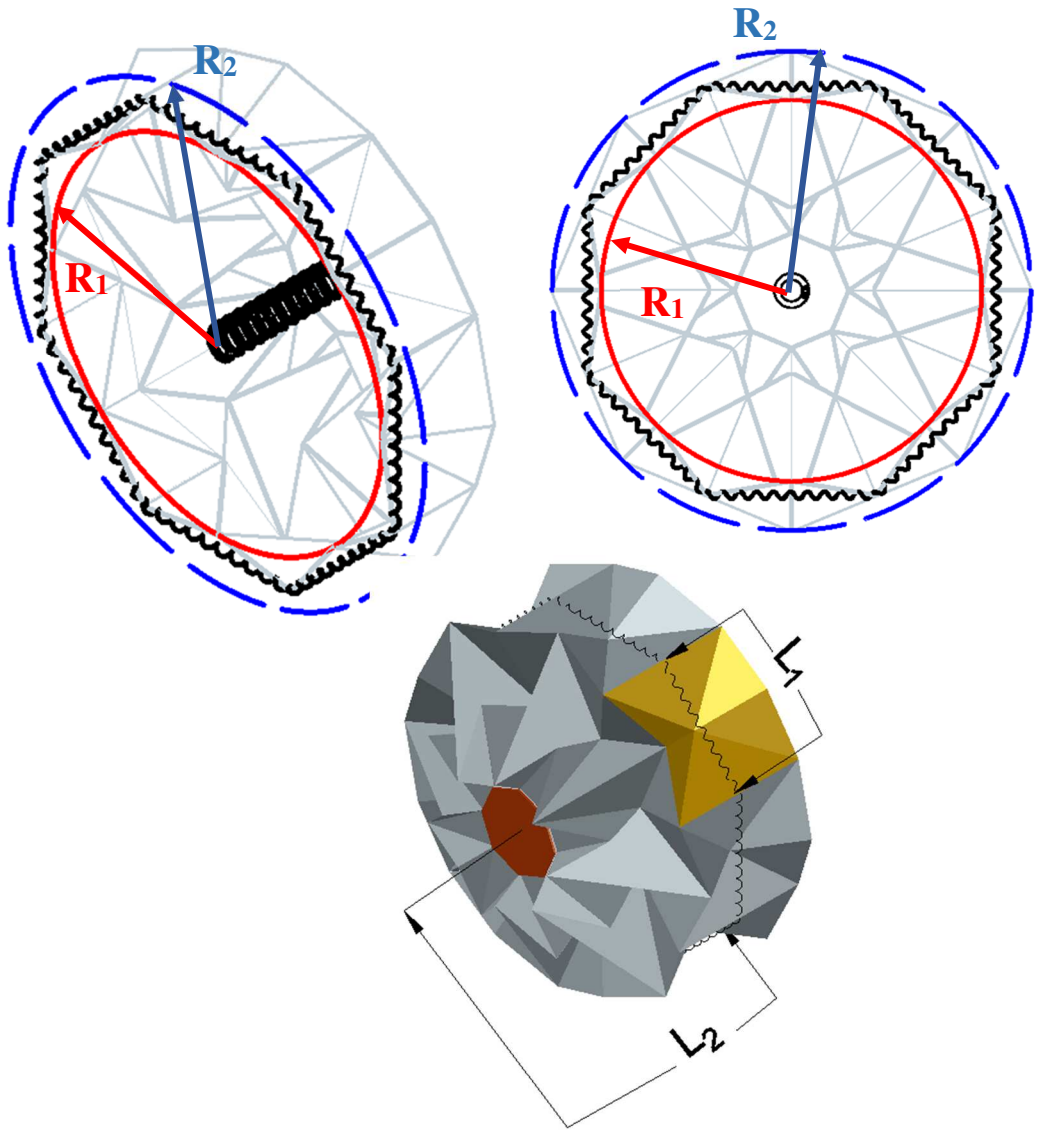

Figure 11: Origami wheel geometric characteristics. Perspective view of the origami wheel showing the inner and the outer radius (superior panel, left); front view of the origami wheel (superior panel, right); and a view of the structure showing the actuators length and its position in the origami wheel (inferior panel).

2.3 – From unit cell to the whole structure

Origami kinematics analysis can be performed by considering two view plans presented in Figure 12: *XZ* plan, from which it is possible to observe radial or rotational symmetry; and *YZ* plan, which shows the longitudinal or reflection symmetry.

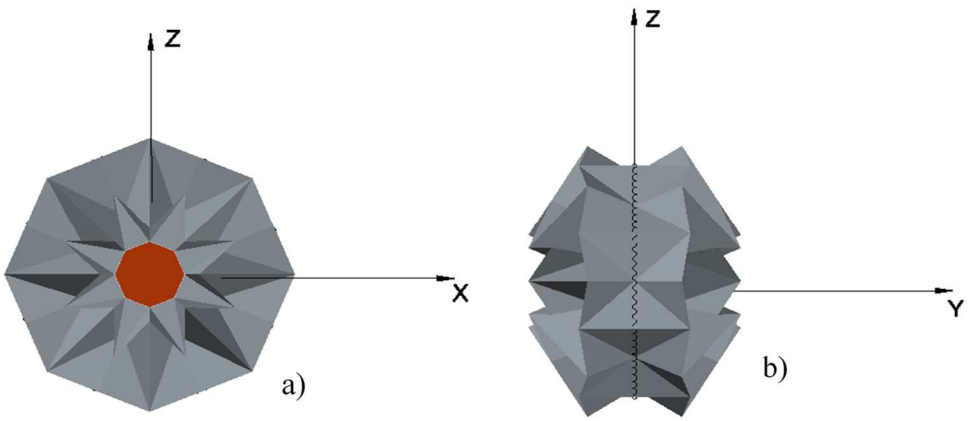

Figure 12: Plan views of the origami wheel.

Besides angles α and θ that describe the opening/closure process of the unit cell, the angles β and γ are associated with the opening/closure process of the entire structure. These angles are related to each other, and this section begins with the study of this relation. Figure 13 shows the origami wheel and the position for the trapezoidal pyramid used to obtain the angle relations. Note that angles β and γ are both related to the position of the cells on the tips (near the acrylic plate), and it is a function of the number of cells (N) that compound the origami wheel column.

The acrylic plate length is given by $l_p = 2r\,\sin(\pi/N)$, and the bases of the trapezium of $BB'B_{P_1}B'_{P_1}$ is a function of R_2, the unit cell size and the number of cells, given by $\overline{BB'} = R_2\,\sin(\pi/N)$ and $\overline{B_{P_1}B_{P_1}'} = (R_2 - 2b\,\sin\beta)\sin(\pi/N)$.

Besides that, since symmetrical behavior is established, it is possible to observe that $\overline{BB'} \,//\, \overline{B_{P1}B'_{P1}} \,//\, \overline{B_{P2}B'_{P2}}$.

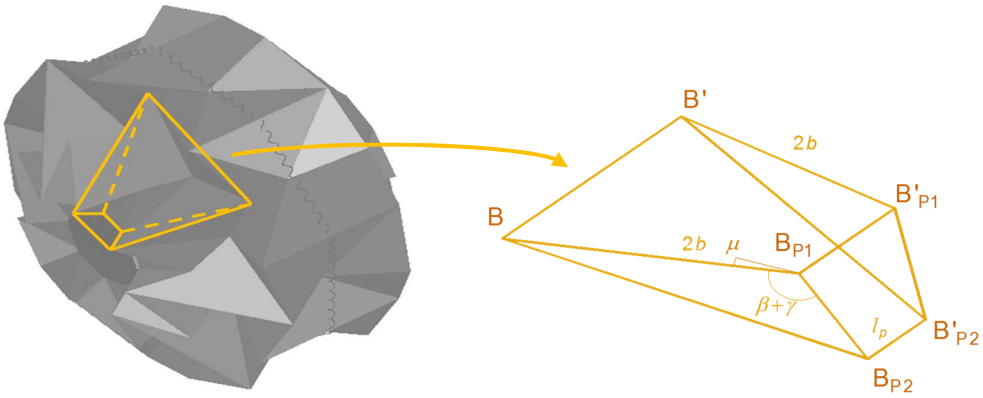

Figure 13: Trapezoidal pyramid defined to characterize origami wheel geometry.

Under these assumptions, the final relation between β and γ is established as $\sin\gamma = \cos\beta \Big/ \sqrt{1 - \sin^2\beta \sin^2(\pi/N)}$, and it is represented in Figure 14. Note that, by increasing N, the angles β and γ tend to be complementary. By using N=8, the maximum error considering the complementary assumption is around 2.5%, ensuring that $\beta + \gamma \approx \pi/2$, a value assumed by Lee (2013).

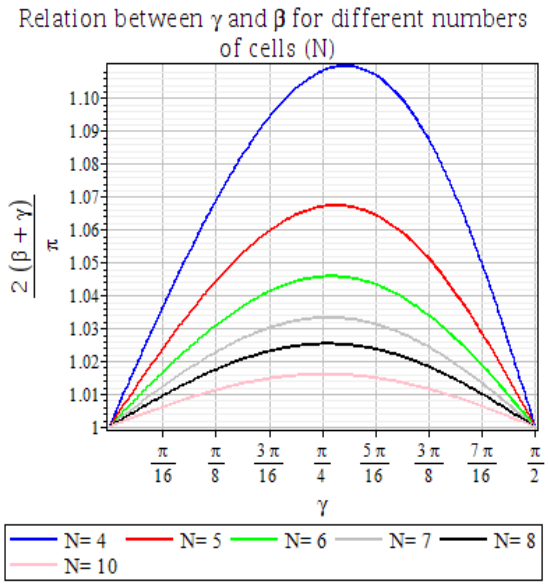

Figure 14: Relation between angles β and γ that define the geometric characteristics of the origami wheel.

Figure 15 allows one to observe some important variables and parameters for origami modeling: SMA spring length (L_1), the half-length of the elastic passive spring (L_2), the acrylic plate dimension ($2r$) (circle diameter circumscribed in a regular octagon), small radius (R_1) and large radius (R_2). Note that the idea of small/large radius is related to the *Z* coordinate of the vertices of the unit cell, representing the inner/outer radius. Figure 15-a and 15-c show the origami *XZ* and *YZ* plan views while Figure 15-b and 15-d show the equivalent mechanism that represents the origami motion.

By considering the complementary condition described and assuming that $c=b/2$, it is possible to obtain the relations for the origami as follows, projecting the lengths on axis *X*, *Y* and *Z*.

$$L_2 = b\,\sin\alpha + 2b\,\cos\beta - \tfrac{b}{2}\sin\beta \tag{6}$$

$$R_2 = r + 2b\,\sin\beta + \tfrac{b}{2}\cos\beta = R_1 + b\,\cos\alpha \tag{7}$$

$$L_1 = 2a\,\sin\theta \tag{8}$$

$$R_1 = a\left(\sin\theta \big/ \tan\tfrac{\pi}{8} - \cos\theta\right) \tag{9}$$

$$R = L_1 \big/ 2\sin\tfrac{\pi}{8} \tag{10}$$

Note that there are two expressions for R_2, both presented in Equation (7). These two forms can be obtained considering either the decomposition of the red edges of Figure 15, leading to the second right hand side expression, or the decomposition of the blue edges of Figure 15, leading to the first right hand side expression. Both decompositions are made on *Z*-axis.

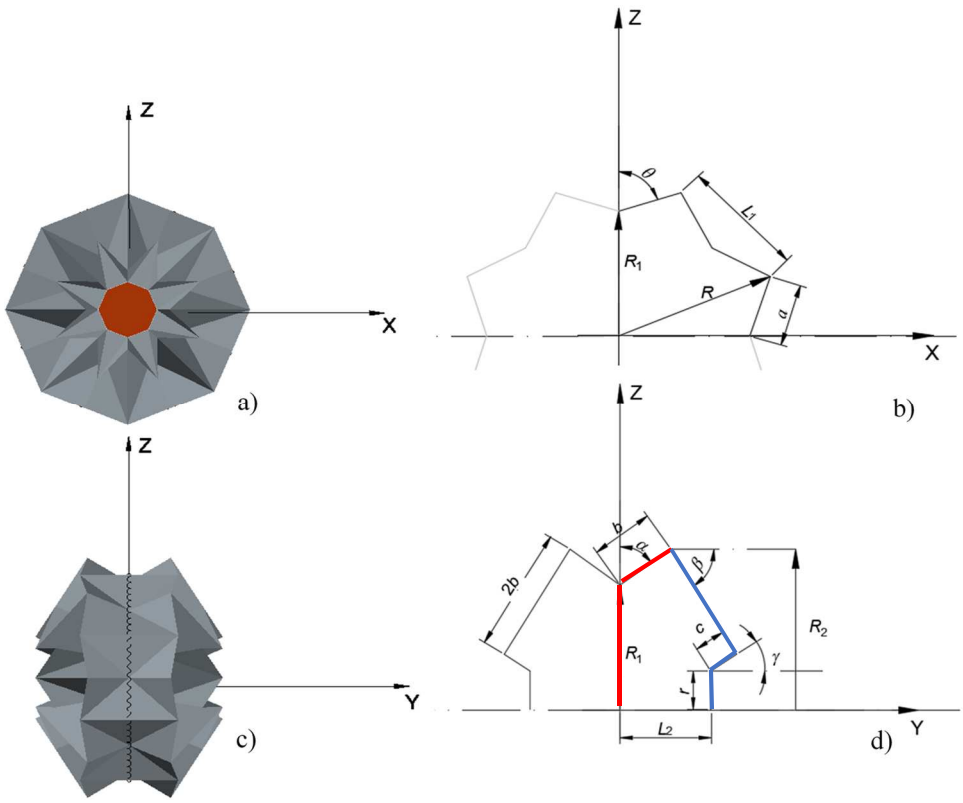

Figure 15: Plan views for the origami wheel and the equivalent mechanism: (a) plan XZ – radial symmetry; (b) equivalent mechanism for plan XZ; (c) plan YZ - longitudinal or axial symmetry; (d) equivalent mechanism for plan YZ.

Based on geometric relations, an explicit relation between L_2 and L_1 is established by solving the system of equations (5 –10), leading to a function $L_2 = g(L_1)$. It is also possible to explicit R_1 and R_2 as functions of L_1. Figure 16 shows graphical representations of these relations considering $r = 0.04$m, $b = 0.065$m and $\lambda = \pi/4$ (a square unit cell). For these values, the range of feasible for constructive reasons is $L_1 \in [0.0555, 0.1225]$ m. Figure 16-a shows the curve $L_2 = g(L_1)$ and Figure 16-b shows the curves of the large radius, R_2, and small radius, R_1, as a function of L_1.

It should be pointed out the different configurations of the origami wheel: P_0 represents the reference construction configuration, where the origami wheel is not completely opened, and the actuators are mounted; P_1 represents the minimum radius configuration, where the origami wheel is completely closed; P_2 represents the maximum radius configuration, where the origami wheel is completely open. Table 1 presents origami wheel configuration characteristics. The percentage variation is related to the difference between the limit configurations, P_1 and P_2, using configuration P_0 as a reference. Note that the origami reduces dramatically its shape, reducing by almost half the large radius (R_2).

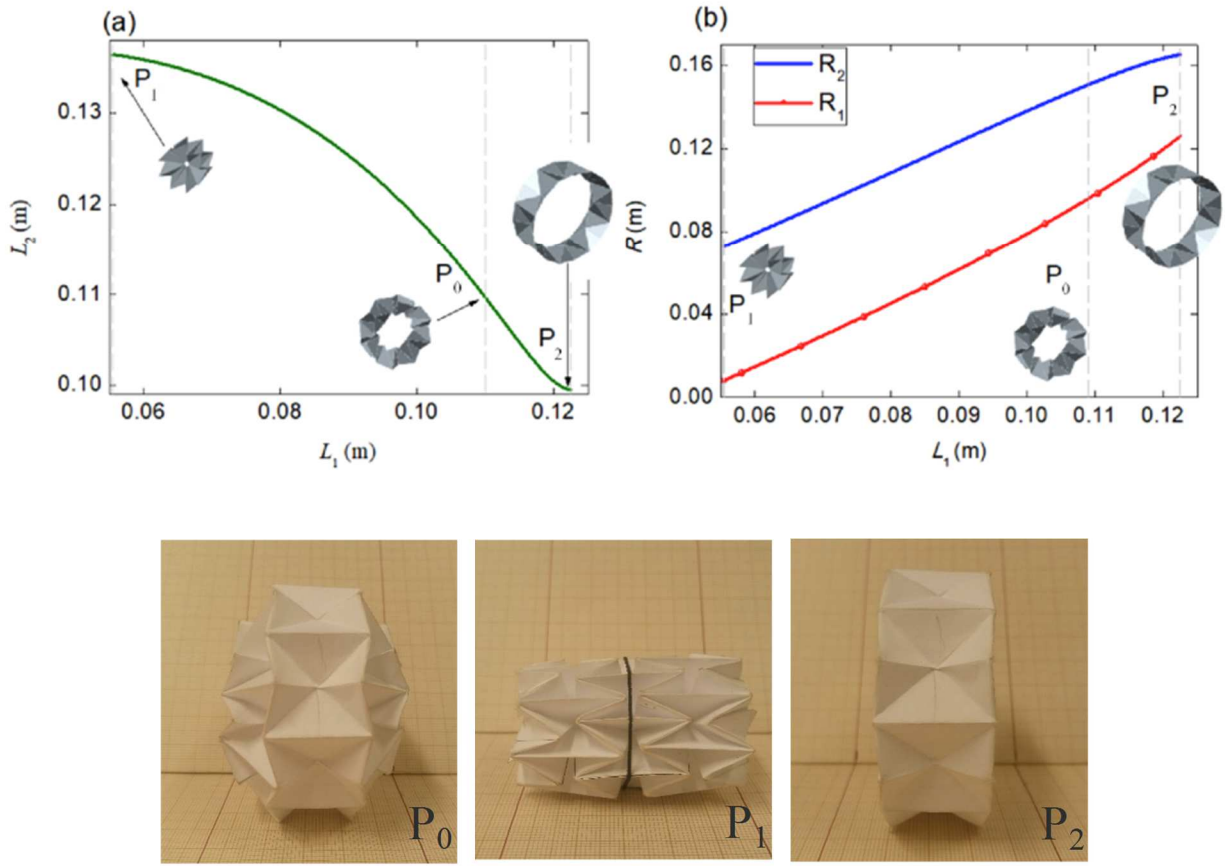

Figure 16: Origami wheel geometric relations. (a) Length of the passive elastic spring as a function of the length of the SMA spring. (b) Small and large radii as a function of the length of the SMA spring. Detailed pictures of the different configurations of the origami wheel are also presented.

Table 1: Configurations of the origami wheel for b = 0.04m and a = 0.065m

	(°)			(m)			
P	α	β	θ	L_1	L_2	R_2	R_1
1	52.98	55.14	70.44	0.1225	0.0995	0.1652	0.1261
2	5.75	0.17	25.27	0.0555	0.1364	0.0729	0.0082
3	32.82	41.72	56.98	0.1090	0.1106	0.1508	0.0962
Maximum variation				0.0670	0.0369	0.0923	0.1179
				61.5%	33.4%	61.2 %	122.6%

Another interesting definition for geometrical modeling is the use of spring displacement instead of its length. Hence, assuming that the reference configuration is that at which the SMA spring is free of both stress and strain, $L_1^0 = 0.089\text{m}$, the SMA length can be written as $L_1 = L_1^0 + u$, where u is the SMA displacement. The same assumption can be made for the elastic passive spring: $L_2 = L_2^0 + u_E$, where u_E is the elastic spring displacement and $L_2^0 = g(L_1^0 + u_0)$, where u_0 is the initial displacement applied to the SMA. Note that the reference configuration for the elastic spring, free stress and strain condition, is the reference configuration P_0, which means that $u_0 = 0.02\text{m}$.

3 EQUATIONS OF MOTION

Origami wheel dynamical model is established by developing the equations of motion based on the kinematics analysis that, due to symmetry assumptions, defines a one-degree of freedom system. Therefore, a reduced-order 1DOF model is able to describe origami dynamics.

Initially, it is necessary to describe the thermomechanical behavior of SMA by considering a constitutive model. This paper considers a polynomial constitutive model to establish a stress-strain-temperature relation (Falk, 1980; Paiva & Savi, 2006). This one-dimensional model assumes a sixth-order polynomial free energy. Based on that, three macroscopic phases are treated: austenite, A, stable at elevated temperatures, and two variants of the martensite, M^+ and M^-, induced by tension and compression, respectively. The form of the polynomial is such that at high temperatures, the free energy has only one minimum at vanishing strain; and at low temperatures, it has two minima at non-vanishing strains and a maximum at the vanishing strain, being mathematically expressed by Ψ_{SMA}, the SMA potential energy:

$$\Psi_{SMA} = \frac{c_1(T-T_M)\varepsilon^2}{2} - \frac{c_2\varepsilon^4}{4} + \frac{c_3\varepsilon^6}{6} \tag{11}$$

where c_1, c_2 and c_3 are model parameters and T_M represents the temperature bellow which the martensitic phase is stable.

The description of force-displacement-temperature relation of SMA helical springs may be related to different hypothesis for the phase transformation through the spring cross section. Essentially, three regions on the wire cross-section need to be considered: a linear-elastic region where a single phase is observed; a region where phase transformation occurs; and a transition region between the first and the second regions. The phase transformation region is not

homogeneous itself since it is a stress induced transformation and therefore, follows the stress distribution through the wire.

Aguiar *et al.* (2010) showed that it is possible to neglect these three regions assuming the homogeneous hypothesis. Based on this, there is only one region, meaning that phase transformation is homogeneous through the cross section. This assumption produces results that are in close agreement with experimental data. Enemark *et al.* (2016) presented deeper explanations about spring description considering the torsion-bending behavior of the wire. Under this assumption, different theories are proposed to deal with the spring modeling. The main conclusion is that a single point model is usually enough to represent the global behavior of the SMA spring. In brief, more complex descriptions are necessary when geometrical nonlinearities are preponderant (Savi *et al.*, 2015).

Therefore, homogeneous hypothesis is related to a single point description, making spring force-displacement-temperature relation similar to one-dimensional stress-strain-temperature relations. Under these assumptions, spring description considers a helical spring with N_S coils with diameter D and wire diameter d. The SMA spring restitution force, $F_{SMA} = \frac{\partial \Psi_{SMA}}{\partial u}$, is then given by:

$$F_{SMA} = \frac{\partial r_{SMA}}{\partial u}\left(\frac{\pi d^3}{6D}\right)_{SMA}\left[c_1(T - T_M)r_{SMA} - c_2\left(\frac{d}{\pi D^2 N_S}\right)^3_{SMA} r^3_{SMA} + c_3\left(\frac{d}{\pi D^2 N_S}\right)^5_{SMA} r^5_{SMA}\right] \tag{12}$$

where r_{SMA} is the radius variation $r_{SMA} = R - R^0$, being related to the radial displacement of the mass associated with the SMA actuator. By using Equation (10) and the displacement definition, u, it is possible to write,

$$r_{SMA} = R - R^0 = \frac{L_1}{2\sin\frac{\pi}{8}} - \frac{L_1^0}{2\sin\frac{\pi}{8}} = \frac{u}{2\sin\frac{\pi}{8}} \tag{13}$$

Concerning the passive elastic spring, a linear relation describes the restitution force F_E,

$$F_E = \frac{\partial \Psi_E}{\partial u} = \frac{\partial \Psi_E}{\partial u_E}\frac{\partial u_E}{\partial u} = k_E u_E \frac{\partial u_E}{\partial u} \tag{14}$$

where Ψ_E is the elastic potential energy; $k_E = \left(\frac{Gd^4}{6D^3N}\right)_E$ and G is the shear modulus.

Dynamical model assumes that the origami has a total mass $8m$, such that each SMA actuator is related to a mass m. Besides, each acrylic plate associated with the passive elastic spring

half-length has a mass M. Based on that, it is possible to write the system energy, where Ψ_K is the kinetic energy and Ψ_P is the potential energy, defined as follows:

$$\Psi_K = \frac{8m\dot{r}_{SMA}^2}{2} + \frac{2M\dot{u}_E^2}{2}$$
$$\Psi_P = 8\Psi_{SMA} + 2\Psi_E \tag{15}$$

Note that the expression of u_E can be obtained by rewritten $L_2 = g(L_1)$ as a function of the initial configuration and the SMA spring displacement. Since $u_E = L_2 - L_2^0$ and $u = L_1 - L_1^0$, it is possible to write $u_E = g(L_1) - L_2^0 = g(L_1^0 + u) - L_2^0 = f(u)$.

Using the chain rule on $f(u)$ derivation, it is written:

$$\ddot{u}_E = \frac{d}{dt}\left(\frac{\partial f}{\partial u}\frac{\partial u}{\partial t}\right) = f'\ddot{u} + f''\dot{u}^2 \tag{16}$$

By assuming an additional linear viscous dissipation with coefficient ξ and an external stimulus, $F(t)$, that is assumed to be symmetrically applied through the middle column of the origami wheel, respecting the rotational symmetry, equations of motion are written as follows:

$$\begin{cases} \dot{u} = v \\ \dot{v} = \left(\frac{m}{\sin^2\frac{\pi}{8}} + Mf'^2\right)^{-1}\left[F(t) - 4F_{SMA} - Mf'f''v^2 - \eta ff' - \xi v\right] \end{cases} \tag{17}$$

Table 2 shows mechanical and geometric properties of the origami wheel employed on the numerical simulations. All simulations consider a dissipative system with a viscous damping constant ξ = 1N s/m.

Table 2: Material and system parameters.

m (kg)	M (kg)	T_M (K)	T_A (K)
0.008	0.012	291.4	326.4
G_E (GPa)	d_E (m)	D_E (m)	N_E
30.0	2.0×10^{-3}	30.0×10^{-3}	40
c_1 (MPa/K)	c_2 (MPa)	c_3 (MPa)	d_{SMA} (m)
5	7.0×10^{4}	7.0×10^{6}	1.0×10^{-3}
	N_{SMA}	D_{SMA} (m)	
	10	2.5×10^{-3}	

3.1 Quasi-static analysis

In order to evaluate the model capability to describe the origami behavior, a quasi-static analysis is performed neglecting inertia and dissipation terms. Origami construction is assumed to be performed in such a way that elastic springs are free of tension when the SMA actuator is pre-deformed at the martensitic phase and the origami wheel is in the opened configuration P_0. This means that SMA actuator has a residual strain that can be recovered by heating, and the relaxed spring size is given by L_1=0.089 m.

Initially, force analysis is performed considering the combination of SMA and elastic forces. Figure 17 shows the origami resultant force for four different temperatures: T=288K ($T< T_M$); T = 320K ($T_M < T < T_A$); T= 326.4K ($T=T_A$) and T=353 K ($T>T_A$). SMA-origami system is temperature dependent meaning that it is possible to change the origami wheel configuration with temperature variations. Different equilibrium configurations can be observed at null force conditions ($\sum F=0$) depending on temperature and they can be related with the origami configuration: three configurations for low temperature ($T\leq T_M$); five configurations for intermediate temperatures ($T_M<T<T_A$); and one configuration for higher temperatures ($T\geq T_A$). Note that a reduction on displacement u means a reduction on the origami radius, being associated with the closure of the structure. The increase of SMA temperature by 7 K (from 320 K to 327 K) induces the reduction of the large origami radius (R_2) from 0.147 m to 0.122 m ($A\rightarrow B$ indicated in Figure 17). The maximum radius reduction observed ($C\rightarrow D$ indicated in Figure 17) is around 0.058 m. The total reduction of limit configurations (points $P_2 \rightarrow P_1$ in Figure 16) implies a reduction of about 56%.

Experimental results of Fang *et al.* (2017) considered the radial opening/closure of 3x8 origami wheels built with different thickness. The origami wheel has a large radius of 44mm at the opened configuration and, when radially compressed, its radius decreases to 19mm, which means a reduction of 57%. This allows one to verify the mathematical model developed in the present work, since this is almost the same value calculated.

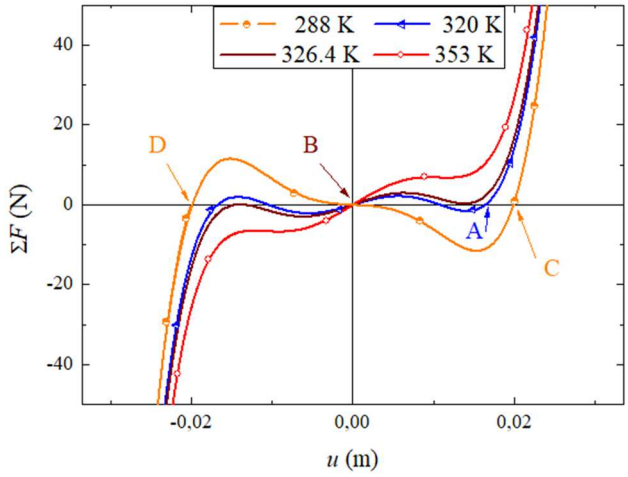

Figure 17: Origami wheel static equilibrium analyzed from the resultant of the involved forces.

Figure 18 shows configuration changes due to temperature variations. Basically, it is presented temperature time history and the origami response representing origami structure path C→B→C, indicated in Figure 17. At initial configuration, T_0=288K, SMA actuators has an initial displacement $u_0 = 0.02\text{m}$, meaning that origami wheel is opened, but not completely. A thermal load from T =288K to T = 373K on SMA (Figure 18-a) recovers SMA residual strain promoting origami closure, as can be noticed by radius reduction (Figure 18-b). Figure 18-c shows SMA and elastic spring displacements during the application of the thermal load. The first vertical dashed line shows the limit temperature at heating process at which opened configuration is stable. At this point (T=T_M), SMA starts phase transformation from martensite to austenite, recovering residual strain and closing the origami wheel. This process takes around 4 seconds. The second and third vertical dashed lines define the start and finish of the origami reopening during the cooling process. This process takes around 15 seconds.

The next section considers dynamical analysis of the origami wheel.

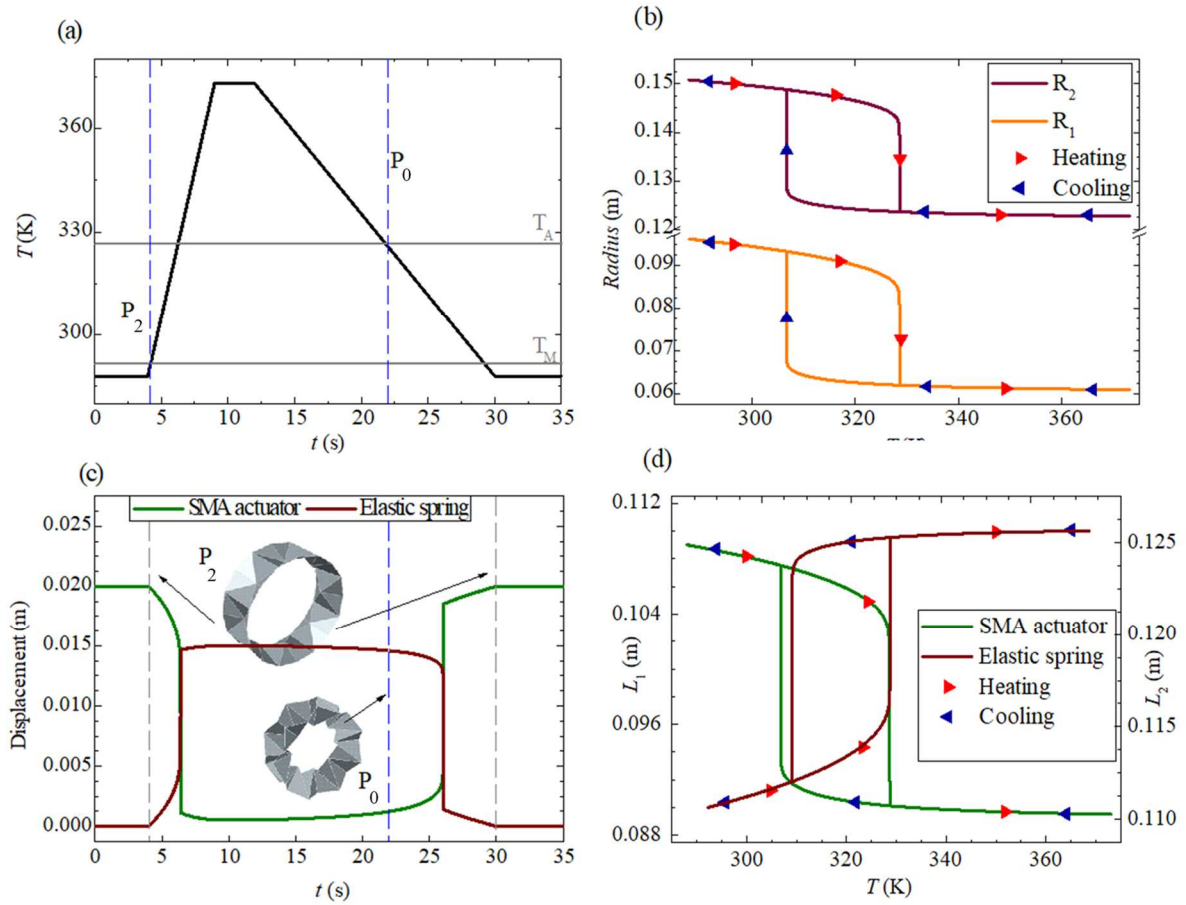

Figure 18: Origami wheel quasi-static behavior due to temperature changes. (a) Thermal load; (b) large and small radii evolution during heating/cooling process; (c) displacement of the elastic spring and of each SMA actuator; (d) actuator lengths.

4 DYNAMICAL ANALYSIS

Dynamical analysis of the origami wheel is now in focus considering perturbations represented by mechanical and thermal loads. It is assumed that origami wheel is subjected to a harmonic mechanical load (green line in Figure 19), with small perturbations that could be related to floor irregularities. These perturbations can be represented by harmonic functions as a Fourier series. In this regard, mechanical loading process is represented as a sum of two sine functions of amplitudes δ_1 and δ_2, and frequencies ω_1 and ω_2.

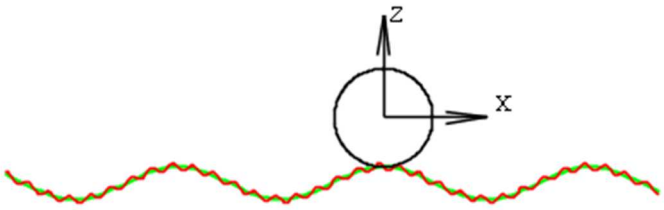

Figure 19: Representation of the perturbed mechanical load acting on origami wheel.

$$F(t) = \delta_1 \sin(\omega_1 t) + \delta_2 \sin(\omega_2 t) \tag{18}$$

Thermal load perturbation is related to environmental temperature oscillation, and its influence on the structure response is investigated. This perturbation is represented by a sine fluctuation of amplitude δ_T, and frequency ω_T, around the nominal temperature, T_N, defined by the following equation,

$$T(t) = T_N + \delta_T \sin(\omega_T t) \tag{19}$$

Numerical simulations are carried out to investigate the origami nonlinear dynamics employing the fourth-order Runge-Kutta method. The structure of equilibrium points is analyzed from basins of attraction presented in Figure 20, built from free vibration analysis of the dissipative system with different initial conditions. Each equilibrium point structure is associated with forces acting on the origami, presented in Figure 17, representing distinct origami wheel configurations, showed in Figure 20-a. Figure 20-b shows a situation where $T<T_M$, with three equilibrium points (two stable and one unstable) that can be reached changing initial conditions. By increasing the temperature for intermediate values ($T_M<T<T_A$), the system changes from three to five equilibrium points (three stable and two unstable), as can be seen at Figure 20-c. By increasing the temperature above T_A, stable points get closer until they coalesce to each other. This causes a change from five equilibrium points to one stable equilibrium point (Figure 20-d). Depending on initial conditions, it is possible to reach a different configuration, changing the origami wheel radius.

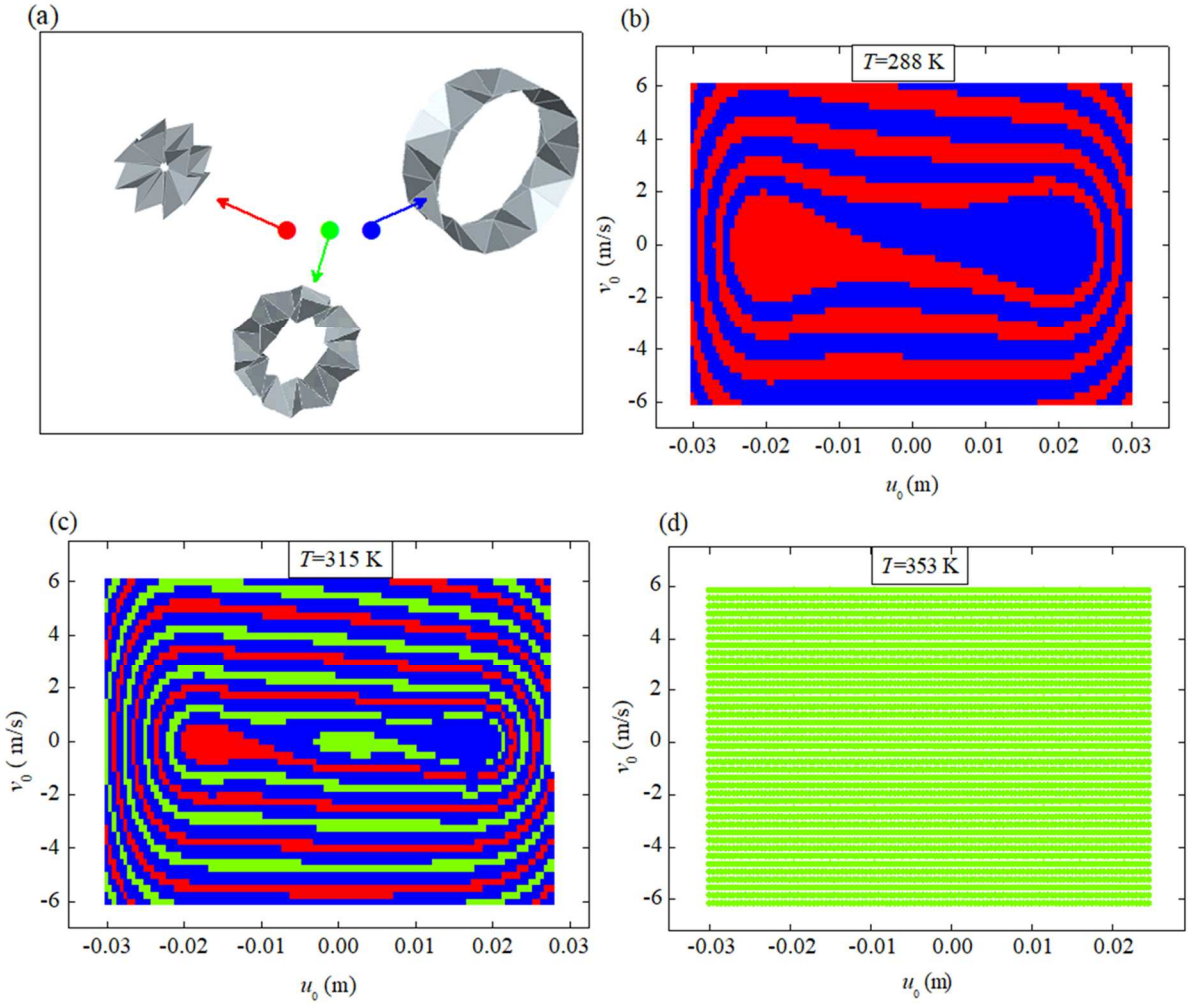

Figure 20: Origami wheel basins of attraction. (a) Configuration for the three stable positions and its color representation; (b) basin of attraction for $T<T_M$; (c) basin of attraction for $T_M<T<T_A$; (d) basin of attraction for $T>T_A$.

Origami slender characteristic is associated with a rich dynamic with strong sensitivity to either parameter changes or initial conditions. In this regard, it is important to have a deep comprehension of the origami wheel nonlinear dynamics, evaluating high periodic, quasi-periodic and chaotic behaviors.

In order to perform a global analysis of the origami response, bifurcation diagrams are built varying forcing amplitude perturbation δ_2, keeping a constant frequency ω_2 = 300rad/s, for δ_1 = 10N and ω_1 = 200rad/s. The objective of this analysis is to evaluate system response under perturbations that can represent soil roughness, with a constant frequency (ω_2=300 rad/s). Different temperature ranges are analyzed: T = 288K ($T < T_M$), T = 315K ($T_M < T < T_A$), and T = 327K ($T > T_A$). Figure 21 shows bifurcation diagrams varying amplitude from zero (δ_2=0, unperturbed excitation forcing) to 1.2N. Note that for the intermediate temperatures (T=315K) the chaotic response disappears when the perturbation increases, changing to a period-2 response (Figure 21-b). By considering low

temperature behavior (T=288K), the perturbation growth tends to increase the response complexity, becoming chaotic (Figure 21-a). Under this condition, bifurcation diagram shows bifurcations and crisis. For δ_2 smaller than 1.1 N, the system presents a period doubling, from period-1 to period-4 response. For δ_2 > 1.1N, a crisis phenomenon is observed, presenting sudden changes from a periodic response to a chaotic-like behavior. For high temperature (Figure 21-c), when austenite is stable (T=320K > T_A), the system has a period-2 behavior for the perturbed case ($\delta_2 \neq 0$) and a period-1 response for the unperturbed case (δ_2=0).

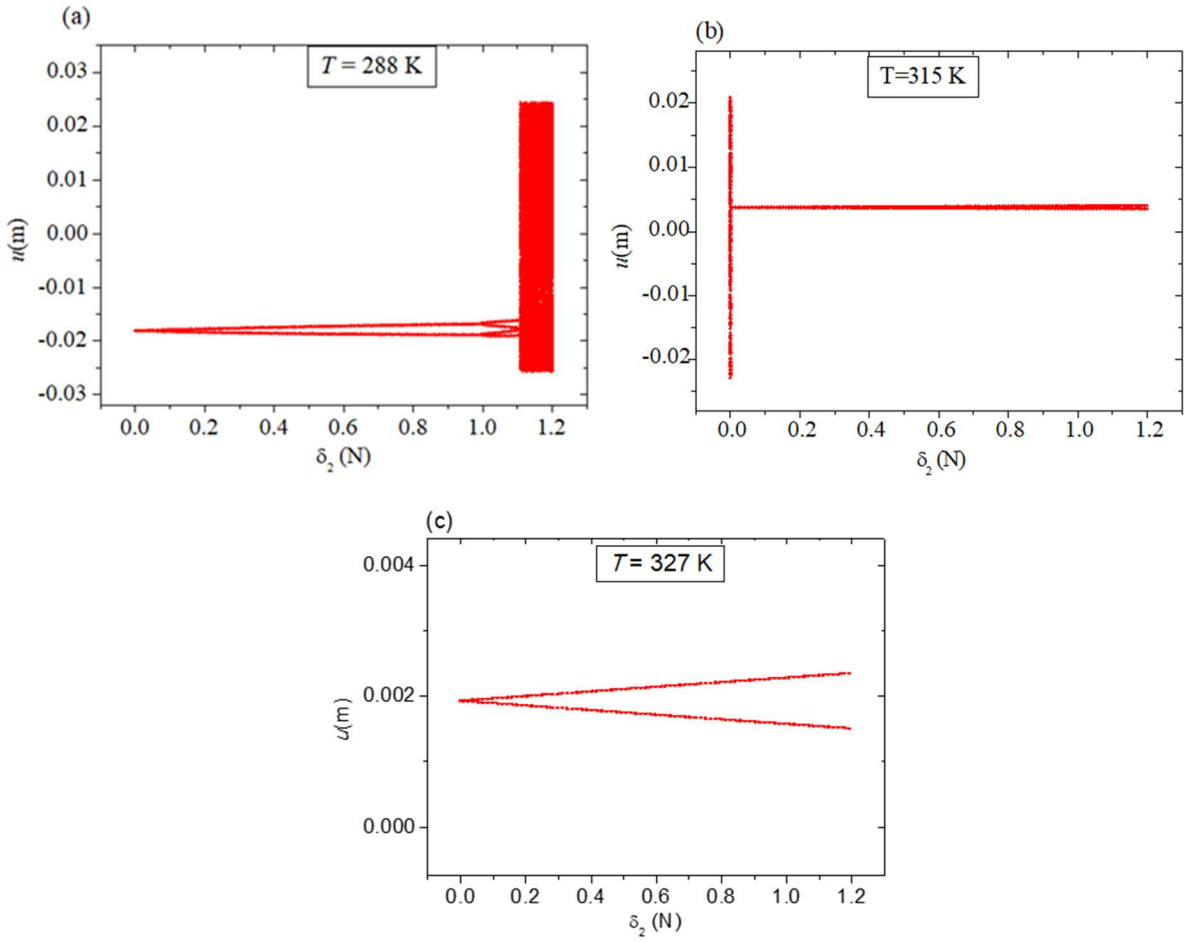

Figure 21: Origami bifurcation diagrams varying perturbation forcing amplitudes: (a) T=288K ($T < T_M$); (b) T = 315K ($T_M < T < T_A$); (c) T=327K ($T > T_A$).

The influence of the external force perturbation (or soil roughness) can be better understood in the sequence. Initially, it is considered a forcing amplitude δ_1=10N and ω_1=200rad/s with a constant low temperature T = 288K (Figure 22-a), without perturbation. Under this condition, origami presents a period-1 behavior, oscillating around the closed configuration with small oscillation amplitude, as shown in Figure 22-b, which presents phase space together with Poincaré section.

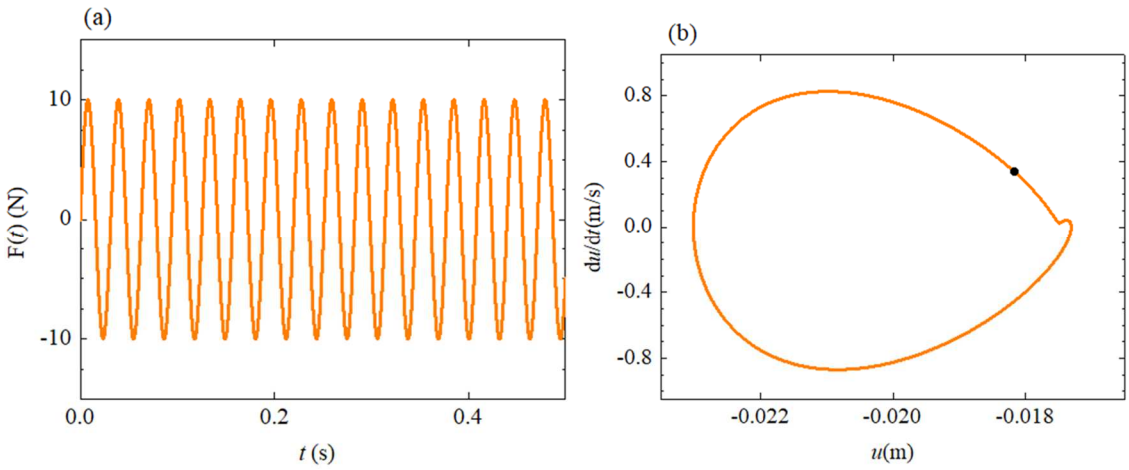

Figure 22: Origami response subjected to mechanical forcing (δ_1=10 N, ω_1=200 rad/s) at T=288 K. (a) Mechanical load); (b) phase space and Poincaré section.

A perturbation is now introduced into the system, considering δ_2=1.5N and ω_2=300rad/s. Figure 23-a shows the original and the perturbed excitations. Under this new condition, origami presents a chaotic motion, which is dramatically different when compared with the previous one. Figure 23-b presents phase space together with Poincaré section that shows a strange attractor. Chaotic behavior is confirmed by the Lyapunov exponents estimated using Wolf *et al.* (1985) algorithm: {60, −80}. The use of Kaplan-Yorke conjecture points to a fractal dimension of 1.737. Figure 23-c shows a phase space identifying some regions associated with stable equilibrium point configurations (similar to Figure 20). Note that origami presents oscillations around several configurations, resulting in large radius variations. This kind of behavior represents an important issue to be evaluated during the design stage since it can be related to unexpected oscillations or related to the structure integrity once high rate of folding process can induce damage on the creases.

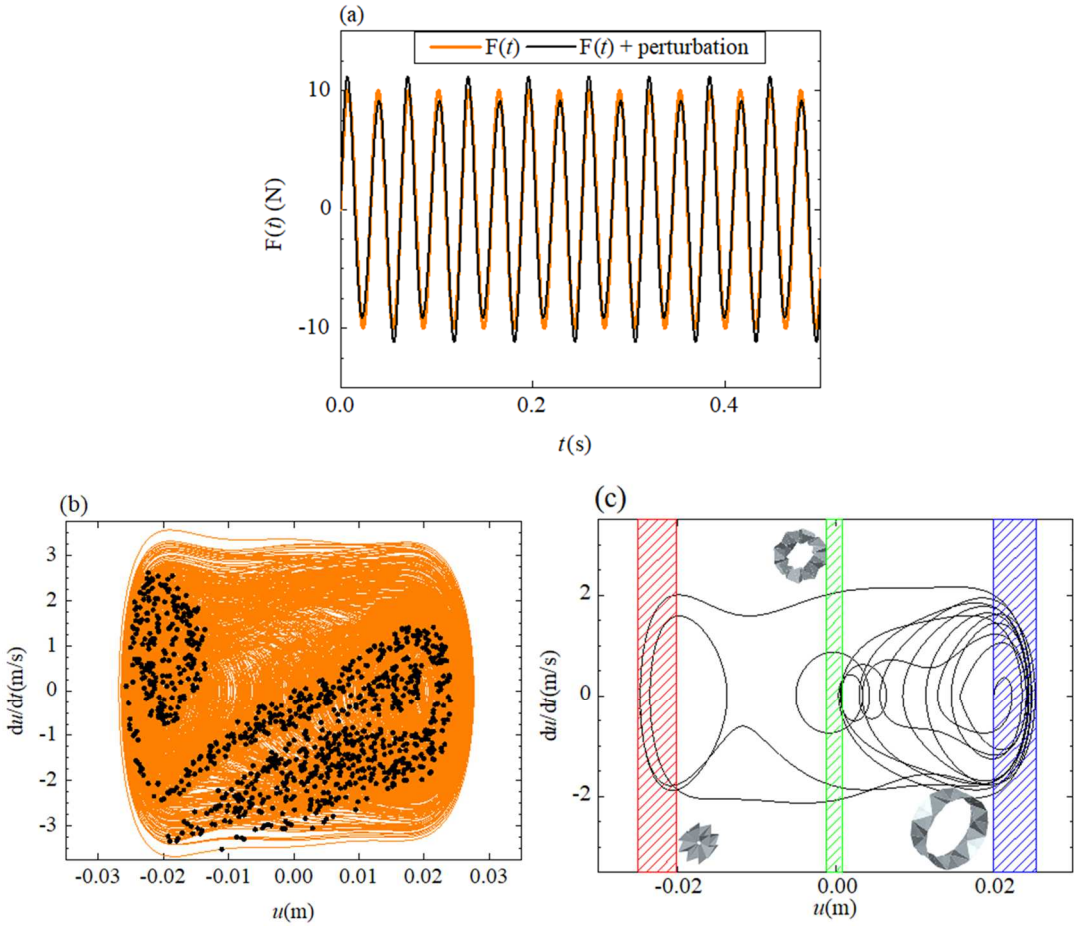

Figure 23: Origami response to a perturbed mechanical load at T=288 K. (a) Mechanical loading process (without and with perturbation); (b) phase space and strange attractor; (c) origami configurations.

Besides mechanical fluctuations, thermal fluctuations also influence origami response. In order to show this kind of behavior, consider a case where the origami is subjected to an external force (δ_1=10 N, ω_1=200 rad/s) at T=288K, case discussed in Figure 22. Thermal perturbations are now introduced, being represented by thermal oscillation: δ_T = 2K and ω_T =100 rad/s. Under this new condition, thermal oscillation induces a transient chaos that stabilizes in a periodic steady state (Figure 24). Figure 24-a shows the time response evolution of the SMA displacement where the origami starts with a transient chaos and stabilizes in a period-2 response approximately after 22 seconds (blue line). During the chaotic response, the structure presents large oscillations, changing between all possible shapes (from completely opened to completely closed). Figure 24-b presents phase spaces for the whole period, showing the same behavior. Figure 24-c presents the chaotic saddle during transient period, while Figure 24-d shows the periodic steady-state stabilized response

where the origami oscillates around the closed configuration. Note that this period-2 response is different from the one obtained for the unperturbed case, period-1 response showed in Figure 22.

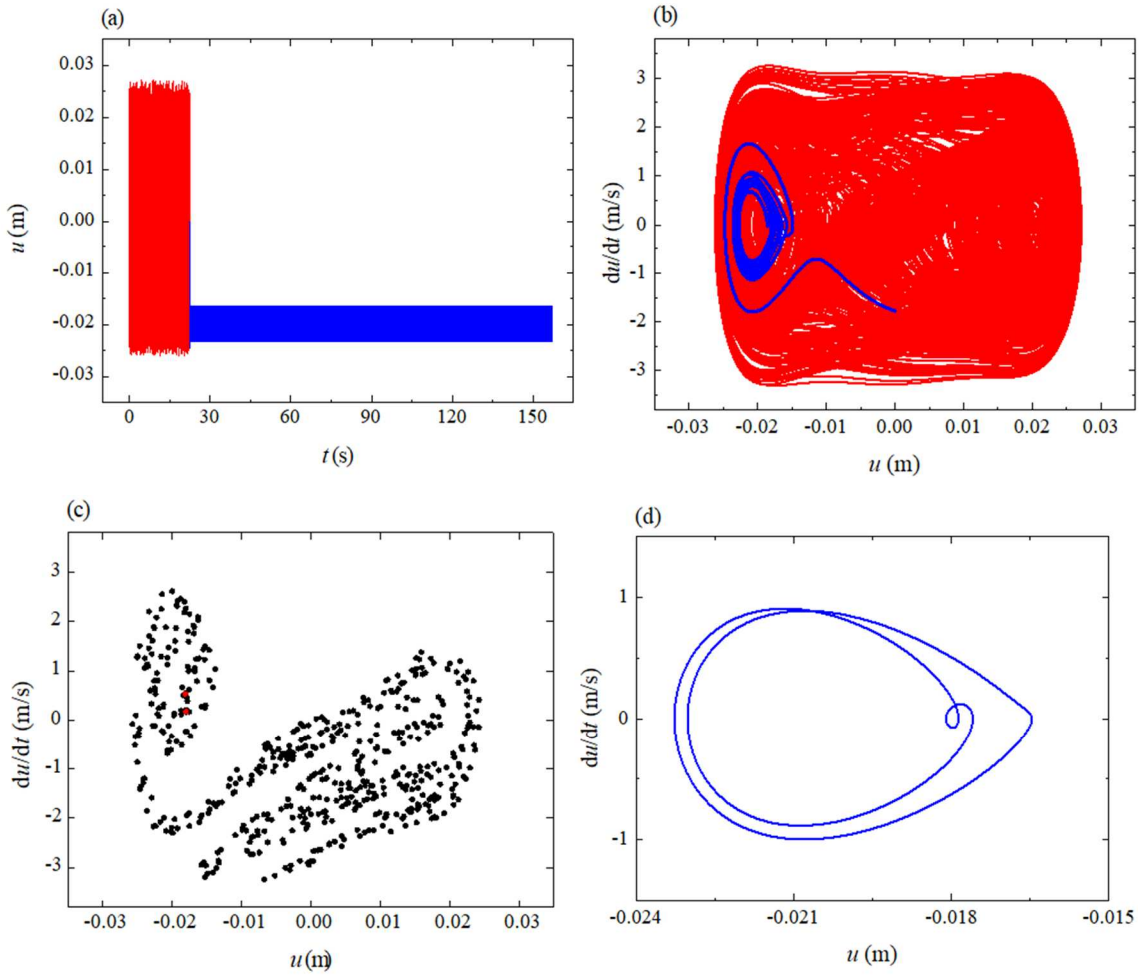

Figure 24: Origami response subjected to thermal fluctuation presenting a transient response, represented by a red line, while steady-state response is represented by a blue line.

(a) SMA displacement time history; (b) phase space; (c) Poincaré section associated with transient chaos (chaotic saddle); (d) periodic steady-state phase space.

Geometric origami alterations is now of concern in order to evaluate its influence on system dynamics. The preceding analysis treats a squared unit cell, which means that $\lambda = \pi/4$. Now, the unit cell is changed for a rectangle pattern, $\lambda=\pi/3$. The new origami is subjected to the same mechanical loads presented in Figure 23 (δ_1 = 10N and ω_1 = 200rad/s, with a perturbation δ_2 = 1.5N and ω_2 = 300rad/s), which presents a chaotic behavior for the square unit cell. The rectangle unit cell changes the chaotic motion to a period-2 response. Figure 25 presents both cases, showing that the same waterbomb pattern can have a completely different response, characterizing a strong parameter dependence on system dynamics.

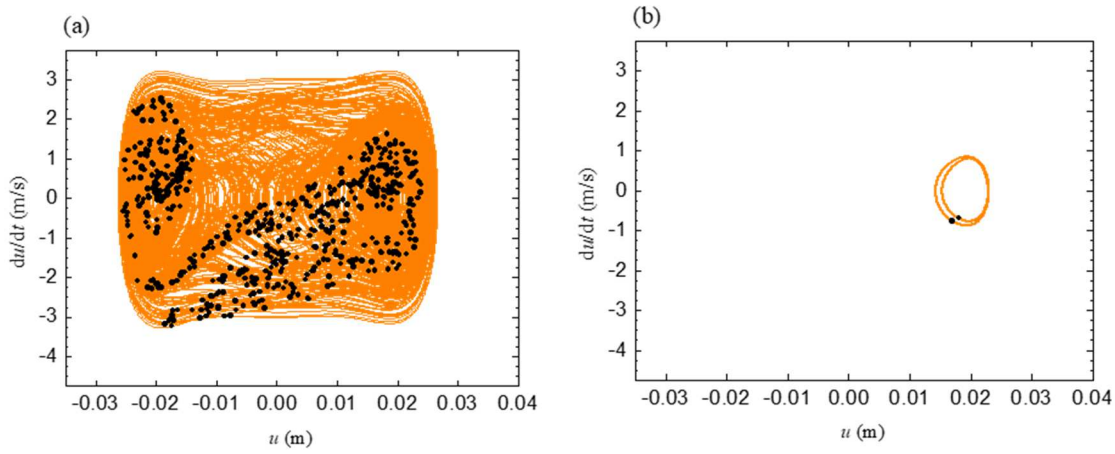

Figure 25: Origami response subjected to a mechanical load for two different geometric characteristics: (a) chaotic response of a square unit cell ($\lambda = {}^{\pi}/_{4}$); (b) periodic response of a rectangle unit cell ($\lambda = {}^{\pi}/_{3}$).

5 CONCLUSIONS

This paper deals with the dynamical analysis of an origami wheel actuated by shape memory alloy actuators. Based on symmetry hypothesis, a reduced-order one-degree of freedom model is proposed to represent the system dynamics. A polynomial constitutive model is employed to describe the thermomechanical behavior of the SMAs and homogeneous phase transformation hypothesis is adopted to describe spring behavior. Equations of motion have a strong nonlinear system related to both geometrical and constitutive nonlinearities. The reduced-order model is able to capture the general origami wheel behavior, being capable of reproduce configuration change, representing the opening/closure process. Besides, it captures the richness of the dynamical behavior. Operational conditions are investigated considering different thermomechanical loading processes, and critical situations are exploited. Numerical simulations are carried out based on different situations that represent real scenarios, such as soil roughness and thermal fluctuations. Some critical motions are investigated. It is noticeable that either mechanical or thermal loadings can deeply affect the system response and should be properly investigated during the design stage. This means that such a slender structure can be exposed to fatigue failure of the creases when subjected to an opening/closure cycles. Chaotic and high-periodic behaviors can be achieved even with small operational condition changes. Besides, although a thermal field can control origami wheel shape, its dynamical behavior is affected by small perturbations that can increase the complexity of the response, leading to high-periodic or chaotic motions. This sensitivity can also be

exploited using chaos control approach, being possible to reduce the response complexity or even mitigate it with the proper stimulus or with small changes on the parameters of the system for a desired operational condition.

6 ACKNOWLEDGEMENTS

The authors would like to acknowledge the support of the Brazilian Research Agencies CNPq, CAPES and FAPERJ. The Air Force Office of Scientific Research (AFOSR) is also acknowledged.

7 REFERENCES

Aguiar, R. A. A., Savi, M. A. & Pacheco, P. M. C. L. (2010), "Experimental and numerical investigations of shape memory alloy helical springs", *Smart Materials and Structures*, v. 19, n. 2, pp.025008.

Baker, J. E. (1980), "An analysis of the Bricard linkages", in *Mechanism and Machine Theory*, v.15, n.4, pp.267-286.

Belcastro, S. M. & Hull, T. C. (2002), "Modeling the folding of paper into three dimensions using affine transformations", *Linear Algebra Appl.*, v.348, pp.273–282.

Chen, Y., Feng, H., Ma, J., Peng, R. & You, Z. (2016), "Symmetric waterbomb origami", *Proceedings of: Royal Society A: Mathematical, Physical and Engineering Science*, v.472, n. 2190.

Chiang, C. H. (2000), "Kinematics of spherical mechanisms", *Malabar, USA: Krieger Publishing Company*.

DuPont Films. (2003), Mylar Polyester Film Product Information. 2003.

Enemark, S., Santos, I. & Savi, M. A. (2016), "Modelling, characterization and uncertainties of stabilized pseudoelastic shape memory alloy helical springs", *Journal of Intelligent Material Systems and Structures*, v. 27, n.20, pp. 2721-2743.

Falk, F. (1980), "Model free-energy, mechanics and thermodynamics of shape memory alloys", *ACTA Metallurgica*, v. 28, n. 12, pp. 1773–1780.

Fang, H., Zhang, Y. and Wang, K.W. (2017), "Origami-Based Earthworm-Like Locomotion Robots", *Bioinspiration & Biomimetics*, v. 12,n. 6.

Fei, L. J. & Sujan, D. (2013), "Origami theory and its applications: a literature review", *International Journal of Social Behavioral, Educational, Economic and Management Engineering*, v. 7, n. 1, pp. 113–117.

Felton, S., Lee, D. Y., Cho, K. J. & Wood, R. J. (2014), "A passive, origami-inspired, continuously variable transmission", *IEEE International Conference on Robotics and Automation*, pp. 2913–2918.

Gogu, G. (2004), “Chebychev–Grübler–Kutzbach's criterion for mobility calculation of multi-loop mechanisms revisited via theory of linear transformations”, *European Journal of Mechanics - A/Solids*, v. 24, n. 3, pp. 427-441.

Huzita, H. (1989), “Axiomatic development of origami geometry”, *Proceedings of the First International Meeting of Origami Science and Technology*, pp. 143-158.

Kuribayashi, K., Tsuchiya, K., You, Z., Tomus, D., Umemoto, M., Ito, T. & Sasaki, M. (2006), “Self-deployable origami stent grafts as a biomedical application of Ni-rich TiNi shape memory alloy foil”, *Materials Science and Engineering A*, v.419, pp. 131–137.

Lang, R.J. (1996), “A Computational Algorithm for Origami Design”, *Proceedings of the twelfth annual symposium on Computational geometry*, p. 98-105.

Lang, R.J. (2011), “Origami design secrets: mathematical methods for an ancient art”. *CRC Press, Alamo.*

Lee, D. Y., Kim, J. S., Kim, S. R., Koh, J. S. & Cho, K-J. (2013), “The deformable wheel robot using magic-ball origami structure”, *Proc. of the ASME 2013 Int. Design Engineering Technical Conf. & Computers and Information in Engineering Conf.* (IDETC/CIE).

Liu, K. and Paulino, G.H. (2017), “Nonlinear mechanics of non-rigid origami: an efficient computational approach”, *Proceedings of Royal Society A: Mathematical, Physical and Engineering Science*. A 473:20170348.

Ly, C., Krishnaraju, D., Konjevod, G, Yu, H. & Jiang, H. (2014), “Origami based Mechanical Metamaterials”, *Scientific Reports*, v. 4, n. 5979.

Ma, J. & You, Z. (2014), “Modelling of the waterbomb origami pattern and its applications”, *International Design and Engineering Technical Conferences and Computers and Information in Engineering Conference* (IDETC/CIE), v. 5B: 38th Mechanisms and Robotics Conference, n. DETC2014-35073, pp. V05BT08A047.

Merz, R., Prinz, F. B., Ramaswami, K., Terk, M., & Weiss, L. E. (1994), "Shape Deposition Manufacturing," *Proceedings of 1994 Solid Freeform Fabrication Symposium,* Austin, pp. 1-8.

Miyashita, S., Guitron, S., Ludersdorfer, M., Sung, C. R., & Rus, D. (2015), “An untethered miniature origami robot that self-folds, walks, swims, and degrades”, *International Conference on Robotics and Automation*.

Nishiyama, Y. (2012), “Miura folding: applying origami to space exploration”, *International Journal of Pure and Applied Mathematics*, v.79, pp. 269-179.

Paiva, A. & Savi, M. A. (2006), “An overview of constitutive models for shape memory alloys”, *Mathematical Problems in Engineering*, v.2006, Article ID56876, pp.1-30.

Peraza-Hernandez, E. A., Hartl, D. J., Malak Jr, R. J. & Lagoudas, D. C. (2014), “Origami-inspired active structures: a synthesis and review”, *Smart Materials and Structures*, v.23, pp. 094001.

Pesenti, M., Masera, G., Fiorito, F. & Sauchelli, M. (2015), “Kinetic solar skin: a responsive Folding technique*”, Energy Procedia*, v.70, pp. 661-672.

Rodrigues, G.V., Fonseca, L.M., Savi, M.A., Paiva, A. (2017), “Nonlinear dynamics of an adaptive origami-stent system”, *International Journal of Mechanical Sciences*, V. 133, pp. 303-318.

Salerno, M., Zhang, K., Menciassi, A. & Dai, J. S. (2014), "A novel 4-DOFs origami enabled, SMA actuated, robotic end-effector for minimally invasive surgery", *IEEE International Conference on Robotics and Automation (ICRA)*, pp. 2844-2849.

Savi, M.A., Paiva, A., de Araujo, C.J. & de Paula, A.S. (2016), "Shape memory alloys", in Lopes Jr, V., Steffen Jr, V., Savi, M.A., *Dynamics of Smart Systems and Structures: Concepts and Applications*, Springer, pp.155-188.

Savi, M.A., Pacheco, P.M.C.L., Garcia, M.S., Aguiar, R.A.A., Souza, L.F.G. & da Hora, R.B. (2015), "Nonlinear geometric influence on the mechanical behavior of shape memory alloy helical spring", *Smart Materials and Structures*, v.24, n.3, Article 0350122015.

Sorguç, A., Hagiwara, I. & Selçuk, S. (2009), "Origamis in architecture: a medium of inquiry for design in architecture", *METU Journal of the faculty of architecture*, 26:2, pp. 235-247.

Wolf, A., Swift, J. B., Swinney, H. L. & Vastano, J. A. (1985), "Determining Lyapunov Exponents from a Times Series", *Physica D*, v. 16, pp. 285–317.